Numerical Benchmarking of Fluid-Structure Interaction: A comparison of different discretization and solution approaches

Stefan Turek, Jaroslav Hron, Mudassar Razzaq, Hilmar Wobker, and Michael Schäfer

Abstract Comparative benchmark results for different solution methods for fluid-structure interaction problems are given which have been developed as collaborative project in the DFG Research Unit 493. The configuration consists of a laminar incompressible channel flow around an elastic object. Based on this benchmark configuration the numerical behavior of different approaches is analyzed exemplarily. The methods considered range from decoupled approaches which combine Lattice Boltzmann methods with hp-FEM techniques, up to strongly coupled and even fully monolithic approaches which treat the fluid and structure simultaneously.

1 Introduction

In [6] specific benchmark problems have been defined in order to have a well-founded basis for validating and also comparing different numerical methods and code implementations for fluid-structure interaction (FSI) problems. In the present paper numerical results obtained with different FSI solution approaches are presented and discussed. The methods involve different discretization schemes and coupling mechanisms.

The FSI benchmark is based on the widely accepted *flow around cylinder* configuration developed in [7] for incompressible laminar flow and on the setup in [8]. Similar to these configurations we consider the fluid to be incompressible and in the laminar regime. The structure is allowed to be compressible, and its deformations are significant. The overall setup of the interaction problem is such

Stefan Turek, Jaroslav Hron, Mudassar Razzaq, Hilmar Wobker
Institut für Angewandte Mathematik, LS III, TU Dortmund, Vogelpothsweg 87, 44227 Dortmund, Germany, e-mail: stefan.turek@math.tu-dortmund.de

Michael Schäfer
Institut für Numerische Berechnungsverfahren im Maschinenbau, TU Darmstadt, Dolivostr. 15, 64293 Darmstadt, Germany, e-mail: schaefer@fnb.tu-darmstadt.de

that the solid object with an elastic part is submerged in a channel flow. Two cases with a steady and an unsteady solution, respectively, are considered. Results for characteristic physical quantities are provided, facilitating comparisons without the use of complicated graphical evaluations. The provided benchmark computations are the result of collaborative simulations which have been part of the research projects inside of the DFG Research Unit 493 and which are presented as separate contributions to this volume (which also contains a more detailed description of the different used FSI codes). The parameter settings and results can be downloaded from `http://featflow.de/en/benchmarks/cfdbenchmarking/fsi_benchmark.html`.

2 Benchmark configuration

We recall the benchmark configuration defined in [6]. It concerns the flow of an *incompressible Newtonian fluid* interacting with an *elastic solid*. We denote by Ω_t^f and Ω_t^s the domains occupied by the fluid and the solid, resp., at the time $t \geq 0$. Let $\Gamma_t^0 = \bar{\Omega}_t^f \cap \bar{\Omega}_t^s$ be the part of the boundary where the elastic solid interacts with the fluid.

2.1 Fluid properties

The fluid is considered to be *Newtonian*, *incompressible* and its state is described by the velocity and pressure fields $\boldsymbol{v}^f, p^f$. The balance equations are

$$\begin{aligned} \rho^f \frac{\partial \boldsymbol{v}^f}{\partial t} + \rho^f (\nabla \boldsymbol{v}^f) \boldsymbol{v}^f &= \operatorname{div} \boldsymbol{\sigma}^f \\ \operatorname{div} \boldsymbol{v}^f &= 0 \end{aligned} \qquad \text{in } \Omega_t^f. \tag{1}$$

The material constitutive equation is

$$\boldsymbol{\sigma}^f = -p^f \boldsymbol{I} + \rho^f \nu^f (\nabla \boldsymbol{v}^f + \nabla \boldsymbol{v}^{f\mathrm{T}}). \tag{2}$$

The constant density of the fluid is ρ^f and the viscosity is denoted by ν^f.

2.2 Structure properties

The structure is assumed to be *elastic* and *compressible*. Its deformation is described by the displacement $\boldsymbol{u}^s$, with velocity field $\boldsymbol{v}^s = \frac{\partial \boldsymbol{u}^s}{\partial t}$. The balance equations are

$$\rho^s \frac{\partial \boldsymbol{v}^s}{\partial t} + \rho^s (\nabla \boldsymbol{v}^s)\boldsymbol{v}^s = \mathrm{div}(\boldsymbol{\sigma}^s) + \rho^s \boldsymbol{g} \qquad \text{in } \Omega_t^s. \tag{3}$$

Written in the more common Lagrangian description, i.e. with respect to some fixed reference (initial) state Ω^s, we have

$$\rho^s \frac{\partial^2 \boldsymbol{u}^s}{\partial t^2} = \mathrm{div}(J\boldsymbol{\sigma}^s \boldsymbol{F}^{-\mathrm{T}}) + \rho^s \boldsymbol{g} \qquad \text{in } \Omega^s, \tag{4}$$

where $\boldsymbol{F} = \boldsymbol{I} + \nabla \boldsymbol{u}^s$ is the deformation gradient tensor. For further details see for example [1].

The material is specified by the Cauchy stress tensor $\boldsymbol{\sigma}^s$ or by the 2nd Piola-Kirchhoff stress tensor $\boldsymbol{S}^s = J\boldsymbol{F}^{-1}\boldsymbol{\sigma}^s\boldsymbol{F}^{-T}$ via the *St. Venant-Kirchhoff* constitutive law

$$\boldsymbol{\sigma}^s = \frac{1}{J}\boldsymbol{F}\left(\lambda^s(\mathrm{tr}\boldsymbol{E})\boldsymbol{I} + 2\mu^s\boldsymbol{E}\right)\boldsymbol{F}^{\mathrm{T}}, \tag{5}$$

$$\boldsymbol{S}^s = \lambda^s(\mathrm{tr}\boldsymbol{E})\boldsymbol{I} + 2\mu^s\boldsymbol{E}, \tag{6}$$

where $\boldsymbol{E} = \frac{1}{2}(\boldsymbol{F}^{\mathrm{T}}\boldsymbol{F} - \boldsymbol{I})$ is the Green-St. Venant strain tensor.

The density of the structure in the undeformed configuration is ρ^s. The elasticity of the material is characterized by the Poisson ratio ν^s ($\nu^s < 0.5$ for a compressible structure) and by the Young modulus E^s. The alternative characterization is described by the Lame coefficients λ^s and μ^s (the shear modulus):

$$\nu^s = \frac{\lambda^s}{2(\lambda^s + \mu^s)} \qquad E^s = \frac{\mu^s(3\lambda^s + 2\mu^s)}{(\lambda^s + \mu^s)} \tag{7}$$

$$\mu^s = \frac{E^s}{2(1+\nu^s)} \qquad \lambda^s = \frac{\nu^s E^s}{(1+\nu^s)(1-2\nu^s)} \tag{8}$$

2.3 Interaction conditions

The boundary conditions on the fluid-solid interface are assumed to be

$$\begin{aligned} \boldsymbol{\sigma}^f \boldsymbol{n} &= \boldsymbol{\sigma}^s \boldsymbol{n} \\ \boldsymbol{v}^f &= \boldsymbol{v}^s \end{aligned} \qquad \text{on } \Gamma_t^0, \tag{9}$$

where $\boldsymbol{n}$ is a unit normal vector to the interface Γ_t^0. This implies the no-slip condition for the flow, and that the forces on the interface are in balance.

2.4 Domain definition

The problem domain, which is based on the 2D version of the well-known CFD benchmark in [7], is illustrated in Figures 1.

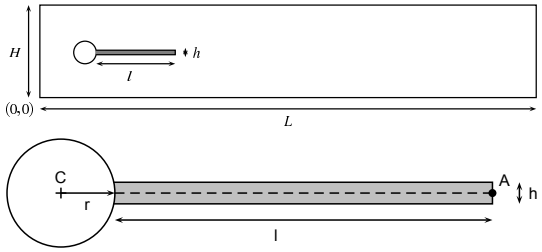

Fig. 1 Computational domain and details of the structure part

The geometry parameters are given as follows (all values in meters):

- The domain has length $L = 2.5$ and height $H = 0.41$.
- The circle center is positioned at $C = (0.2, 0.2)$ (measured from the left bottom corner of the channel) and the radius is $r = 0.05$.
- The elastic structure bar has length $l = 0.35$ and height $h = 0.02$, the right bottom corner is positioned at $(0.6, 0.19)$, and the left end is fully attached to the fixed cylinder.
- The control point is $A(t)$, attached to the structure and moving in time with $A(0) = (0.6, 0.2)$.

The setting is intentionally non-symmetric (see [7]) to prevent the dependence of the onset of any possible oscillation on the precision of the computation.

2.5 Boundary conditions

The following boundary conditions are prescribed:

- A parabolic velocity profile is prescribed at the left channel inflow

$$v^f(0,y) = 1.5\bar{U}\,\frac{y(H-y)}{(H/2)^2} = 1.5\bar{U}\frac{4.0}{0.1681}\,y(0.41-y), \tag{10}$$

  such that the mean inflow velocity is $\bar{U}$ and the maximum of the inflow velocity profile is $1.5\bar{U}$.
- The outflow condition can be chosen by the user, for example *stress free* or *do nothing* conditions. The outflow condition effectively prescribes some reference value for the pressure variable p. While this value could be arbitrarily set in the

incompressible case, in the case of compressible structure this will have influence on the stress and consequently the deformation of the solid. In this proposal, we set the reference pressure at the outflow to have *zero mean value*.

- The *no-slip* condition is prescribed for the fluid on the other boundary parts, i.e. top and bottom wall, circle and fluid-structure interface Γ_t^0.

2.6 Initial conditions

The suggested starting procedure for the non-steady tests was to use a smooth increase of the velocity profile in time as

$$v^f(t,0,y) = \begin{cases} v^f(0,y)[1-\cos(\pi t/2)]/2 & \text{if } t < 2.0 \\ v^f(0,y) & \text{otherwise} \end{cases} \tag{11}$$

where $v^f(0,y)$ is the velocity profile given in equation (10).

2.7 Physical parameters

We consider physical parameters for two different test cases as indicated in Table 1. Defining the Reynolds number by $\mathrm{Re} = 2r\bar{U}/\nu^f$ the two cases correspond to Re=20 and Re=200. FSI1 is resulting in a steady state solution, while FSI3 results in a periodic solution (the numbering refers to the original benchmark definition in [6]).

Table 1 Parameter settings for the FSI benchmarks

	FSI1	FSI3
ρ^s [10^3kg/m^3]	1	1
ν^s	0.4	0.4
μ^s [10^6kg/ms^2]	0.5	2.0
ρ^f [10^3kg/m^3]	1	1
ν^f [10^{-3}m^2/s]	1	1
$\bar{U}$ [m/s]	0.2	2

3 Quantities for comparison

Comparisons will be done for *fully developed flow*, and particularly for *one full period of the oscillation* with respect to the position of the point $A(t)$. The quantities of interest are:

1. The displacements $u_1(t)$ and $u_2(t)$ in x- and y-direction of the point $A(t)$ at the end of the beam structure (see Figure 1).
2. Forces exerted by the fluid on the *whole* submerged body, i.e. lift and drag forces acting on the cylinder and the beam structure together

$$(F_D, F_L)^{\mathrm{T}} = \int_S \boldsymbol{\sigma}^f \boldsymbol{n}\, dS = \int_{S_1} \boldsymbol{\sigma}^f \boldsymbol{n}\, dS + \int_{S_2} \boldsymbol{\sigma}^f \boldsymbol{n}\, dS,$$

where $S = S_1 \cup S_2$ (see Figure 2) denotes the part of the circle being in contact with the fluid and $\boldsymbol{n}$ is the outer unit normal vector to the integration path with respect to the fluid domain.

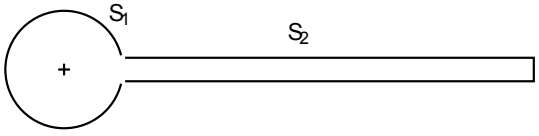

Fig. 2 Integration path $S = S_1 \cup S_2$ for the force calculation

Time dependent values are represented by mean value, amplitude, and frequency. The mean value and the amplitude are computed from the last period of the oscillations by taking the maximum and minimum values, the mean value is taken as average of the max/min values, and the amplitude is the difference of the max/min from the mean:

$$\text{mean} = \frac{1}{2}(\max + \min)$$
$$\text{amplitude} = \frac{1}{2}(\max - \min)$$

The frequency of the oscillations are computed either as $1/T$ with the period time T or by using Fourier analysis on the periodic data and taking the lowest significant frequency present in the spectrum.

4 FSI solution approaches

In the following, a short description of the different approaches, which have been applied in the subsequent benchmark calculations, will be provided. A more detailed

description of the underlying methodology and the corresponding software tools is given as separate contributions to this volume.

Method 1 (Schäfer):

This method involves an implicit partitioned solution approach (see [4, 5] for details). It is realized based on the finite-volume multigrid flow solver FASTEST involving an ALE formulation (hexahedral control volumes, second-order in space and time), the finite-element structural solver FEAP (bilinear brick elements, second-order Newmark time discretization), and the coupling interface MpCCI. For each time step the implicit solution procedure consists in the application of different nested iteration processes for linearization, pressure-velocity coupling, and linear system solving. These are linked by an iterative fluid-structure coupling procedure with structural underrelaxation and displacement prediction.

Method 2 (Rannacher):

Two different solvers have been used in this project, both based on monolithic variational formulations of the FSI problem: (a) one based on a unified Eulerian framework for describing the fluid as well as the structure deformation ("interface capturing") which allows for large structural deformations and topology changes of the flow domain, and (b) for comparison one based on the standard ALE approach ("interface fitting"). The discretization is fully implicit and uses in case (a) the second-order fractional-step-θ scheme and in case (b) the stabilized Crank-Nicolson scheme in time. The spatial discretization is by a conforming finite element Galerkin method on quadrilateral meshes with mixed global and zonal refinement using in case (a) the "equal-order" Q_1^c/Q_1^c Stokes-element for velocity and pressure with pressure and transport stabilization by "local projection", and in case (b) the inf-sup-stable Q_2^c/P_1^d Stokes-element. For the resulting nonlinear algebraic problems in each time step a Newton-like iteration is used (combined with pseudo-time stepping in the stationary test case). The linear subproblems are solved in fully coupled form in case (a) by a multigrid methods with GMRES acceleration, block-ILU smoothing and canonical grid transfers, and in case (b) by a direct solver ("UMFPACK") which allows for up to 10^6 unknowns in acceptable time.

Method 3 (Turek/Hron):

The applied FSI solver is a fully implicit, monolithic ALE-FEM approach. The discretization is based on the classical (nonparametric) Q2/P1 finite element pair, together with the Crank-Nicolson scheme for time stepping. The resulting nonlinear systems are solved by a discrete Newton method, while the linear subsystems

are treated via Krylov-multigrid solvers with smoothing operators of local pressure Schur complement/Vanka-like type with canonical grid transfer routines.

Method 4 (Breuer):

The method relies on a partitioned solution approach. For the fluid flow a finite-volume scheme (FASTEST-3D) is used to discretize the (filtered) Navier–Stokes equations for an incompressible fluid. The discretization is done on a curvilinear, blockstructured body-fitted grid with colocated variable arrangement by applying standard schemes. Linear interpolation of the flow variables to the cell faces and a midpoint rule approximation for the integrals is used to obtain a second-order accurate central scheme. In order to account for displacement or deformation of the structure the Arbitrary Lagrangian-Eulerian formulation is applied. A new partitioned coupling method based on the predictor-corrector scheme often used for LES is prefered. A strongly coupled but nevertheless still explicit time-stepping algorithm results, which is very efficient in the LES–FSI context. For the prediction of the deformation and displacement of the structure, the forces are transferred to computational structure dynamics code, here the finite-element solver Carat provided by the Chair of Structural Analysis of TU Munich. The response of the structure, i.e. the displacements are transferred to the fluid solver. The coupling interface CoMA also developed at TUM is used for this purpose. This interface is based on the Message-Passing-Interface (MPI) and thus runs in parallel to the fluid and structure solver. Presently, the grid adjustment on the fluid side is performed based on a transfinite interpolation.

Method 5 (Krafczyk/Rank):

This method involves an explicit partitioned solution approach. It is realized with the Lattice-Boltzmann flow solver VirtualFluids (VF) and the structural p-FEM solver AdhoC. VirtualFluids is based on an Eulerian grid (cubic, hierarchical, graded FD grids, second-order in space and time). AdhoC discretizes the equations of structural dynamics in space with a Bubnov-Galerkin method utilizing hierarchic ansatz functions while the time domain is discretized with a second-order finite difference scheme (Newmark or generalized alpha). The coupling interface MshPI manages the data transfer on an interface mesh common to all involved solvers. For each time step, the partitioned solution procedure consists of nested substeps. VirtualFluids sends loads via the interface mesh to AdhoC which generates displacements. These, in turn, are then mapped to the fluid grid. The exchange of tractions and displacements is performed only once per structural time step. As the time step for the flow solver is typically smaller than the structural one, VF proceeds for several time steps with an interpolated geometry. It is interesting to note that this setup proved to be stable without the need to perform interfield iterations.

Method 6 (Wall):

For this benchmark scenario we have used our rather "classic" approach selected from the different FSI approaches that we have developed in recent years for solving incompressible fluid flow coupled with large structural deformations. A main ingredient is a strongly coupled, iterative staggered scheme based on [2, 9]. The fluid field uses an ALE formulation, stabilized, quadratic Q2Q2 elements and BDF2 time-discretiyation. The fluid mesh is deformed based on linear-elastic material behavior. The structure is discretized by bi-linear quadrilateral elements with EAS formulation and the generalized-α method for time discretization. Each field is solved implicitly and an iterative procedure over the fields using Aitken relaxation ensures convergence for the interface conditions at the new time step level $n+1$.

Method 7 (Bletzinger):

The coupled problem is solved by a partitioned approach. Three independent software components are combined: in-house codes CARAT++ and CoMA (Computer Aided Research Analysis Tool, Coupling for Multiphysics Analysis) for structural analysis, coupling control and data transfer between non-matching grids, as well as OpenFOAM, an open source finite volume solver. The single field solvers use individual, at the interface non-matching, grids. Implicit coupling schemes based on fixed-point iterations with Aitken relaxation or a quasi-Newton method are used. Different to all other groups the structure has been modelled as a shell (with mid-surface in x-z-plane). Two different shell theories have been applied: a "classical", 5-parameter, Reissner-Mindlin shell model neglecting normal stresses in thickness direction as well as a 7-parameter, 3D solid shell model with a straight thickness director as only kinematic assumption. The difference becomes obvious in FSI1 where a longitudinal Poisson effect due to cross thickness normal stress is evident for the horizontal deformation $u_1 = 1.85 \times 10^{-5}$ (classical shell) or $u_1 = 2.26 \times 10^{-5}$ (solid shell), respectively. All other data match well and show good results in all benchmarks. It is concluded, that shell finite element formulations can be used effectively in FSI analyses and give correct results for structures up to a moderate thickness.

5 Numerical results

The results of the benchmark computations are summarized in Tables 2 and 3 (units are omitted). Indicated are the displacements $u_1(A)$ and $u_2(A)$ in x- and y-direction of the point A as well as the drag and lift forces F_D and F_L. For the unsteady case also the frequencies f_1 and f_2 obtained for the displacements $u_1(A)$ and $u_2(A)$, respectively, are given. The number in the first column refers to the methods given in the previous section. The column "Unknowns" refers to the total number (in space),

i.e., the sum of unknowns for all velocity components, pressure, and displacement components.

Table 2 Results for steady benchmark FSI1.

	Unknowns	$u_1(A)$ $[\times 10^{-5}]$	$u_2(A)$ $[\times 10^{-4}]$	F_D	F_L
1	82722	–	–	14.2770	0.77200
	322338	–	–	14.2890	0.76900
2a	11250	2.4800	7.7800	–	–
2b	19488	2.2821	8.1957	14.2382	0.76481
	29512	2.2793	8.2201	14.2263	0.76420
	51016	2.2733	8.1867	14.2408	0.76400
	93992	2.2710	8.1702	14.2500	0.76392
	179912	2.2700	8.1609	14.2561	0.76389
	351720	2.2695	8.1556	14.2603	0.76388
3	19488	2.2871	8.1930	14.2736	0.76175
	76672	2.2774	8.2042	14.2918	0.76305
	304128	2.2732	8.2071	14.2948	0.76356
	1211392	2.2716	8.2081	14.2949	0.76370
	4835328	2.2708	8.2085	14.2945	0.76374
	19320832	2.2705	8.2088	14.2943	0.76375
5	884736	2.1270	11.0800	14.3179	0.85491
	3538944	2.1990	8.3370	14.3127	0.75138
	14155776	2.2160	8.2010	14.3815	0.75170
6	7059	2.5396	8.8691	14.2800	0.73690
	19991	2.2630	8.2935	14.2970	0.76687
	77643	2.2676	8.2347	14.2940	0.76545
	164262	2.2680	8.2310	14.2940	0.76487
7	217500	2.2640	8.2800	14.3510	0.76351

As a first result for the FSI1 benchmark, which leads to stationary displacement of the attached elastic beam, it is obvious that all applied methods and codes can approximate the same results, at least with decreasing mesh width.

For FSI3, the evaluation of the results is a little bit more difficult: First of all, all schemes show the tendency to converge towards the (more or less) same solution values, at least for increasing mesh level. Although the applied FSI techniques are very different w.r.t. discretization, solver and coupling mechanisms, the FSI3 benchmark setting proves to be a very valuable tool for numerical FSI benchmarking, leading to grid independent results for the prescribed geometrical and parameter settings.

However, also clear differences between the different approaches with regard to accuracy are visible. Particularly for the drag and lift values, which lead to differences of up to order 50%, and also for the displacement values which are in the range of 10% errors. A more detailed evaluation and also more rigorous comparisons w.r.t. the ratio ‘accuracy vs. efficiency’ are therefore planned for the future.

Table 3 Results for unsteady benchmark FSI3.

	Unknowns	Δt	$u_1(A)$ [$\times 10^{-3}$]	$u_2(A)$ [$\times 10^{-3}$]	F_D	F_L	f_1	f_2
1	61318	1.0e-3	-2.54 ± 2.41	1.45 ± 32.80	450.3 ± 23.51	-0.10 ± 143.0	10.90	5.13
	237286	2.0e-3	-2.88 ± 2.73	1.53 ± 34.94	458.6 ± 27.18	2.08 ± 153.1	10.60	5.30
	237286	1.0e-3	-2.87 ± 2.73	1.54 ± 34.94	458.6 ± 27.31	2.00 ± 153.3	10.34	5.91
	237286	5.0e-4	-2.86 ± 2.72	1.53 ± 34.90	458.6 ± 27.27	2.01 ± 153.4	12.16	6.08
	941158	1.0e-3	-2.91 ± 2.77	1.47 ± 35.26	459.9 ± 27.92	1.84 ± 157.7	11.63	4.98
2a	11250	5.0e-3	-2.48 ± 2.24	1.27 ± 36.50	–	–	10.10	5.10
2b	7176	5.0e-3	-2.44 ± 2.32	1.02 ± 31.82	473.5 ± 56.97	8.08 ± 283.8	11.07	5.29
	7176	2.0e-3	-2.48 ± 2.39	0.92 ± 32.81	471.3 ± 62.28	6.11 ± 298.6	10.73	5.35
	7176	1.0e-3	-2.58 ± 2.49	0.94 ± 33.19	470.4 ± 64.02	4.65 ± 300.3	10.69	5.36
	27744	5.0e-3	-2.43 ± 2.27	1.41 ± 31.73	483.7 ± 22.31	2.21 ± 149.0	10.53	5.37
	27744	2.0e-3	-2.63 ± 2.61	1.46 ± 33.46	483.3 ± 24.48	2.08 ± 161.2	10.66	5.43
	27744	1.0e-3	-2.80 ± 2.64	1.45 ± 34.12	483.0 ± 25.67	2.21 ± 165.3	10.75	5.41
	42024	2.5e-3	-2.40 ± 2.26	1.39 ± 31.71	448.7 ± 21.16	1.84 ± 141.3	10.72	5.42
	42024	1.0e-3	-2.53 ± 2.38	1.40 ± 32.49	449.7 ± 22.24	1.61 ± 142.8	10.77	5.44
	42024	5.0e-4	-2.57 ± 2.42	1.42 ± 32.81	450.1 ± 22.49	1.49 ± 143.7	10.79	5.42
	72696	2.5e-3	-2.64 ± 2.48	1.38 ± 33.25	451.1 ± 24.57	2.04 ± 150.6	10.73	5.38
	72696	1.0e-3	-2.79 ± 2.62	1.28 ± 34.61	452.0 ± 25.78	1.91 ± 152.7	10.78	5.42
	72696	5.0e-4	-2.84 ± 2.67	1.28 ± 34.61	452.4 ± 26.19	2.36 ± 152.7	10.84	5.42
3	19488	1.0e-3	-3.02 ± 2.83	1.41 ± 35.47	458.2 ± 28.32	2.41 ± 145.6	10.75	5.37
	19488	5.0e-4	-3.02 ± 2.85	1.42 ± 35.63	458.7 ± 28.78	2.23 ± 146.0	10.75	5.37
	19488	2.5e-4	-3.02 ± 2.85	1.32 ± 35.73	458.7 ± 28.80	2.23 ± 146.0	10.74	5.33
	76672	1.0e-3	-2.78 ± 2.62	1.44 ± 34.36	459.1 ± 26.63	2.41 ± 151.3	10.93	5.46
	76672	5.0e-4	-2.78 ± 2.62	1.44 ± 34.35	459.1 ± 26.62	2.39 ± 150.7	10.92	5.46
	76672	2.5e-4	-2.77 ± 2.61	1.43 ± 34.43	459.1 ± 26.50	2.36 ± 149.9	10.93	5.46
	304128	1.0e-3	-2.86 ± 2.70	1.45 ± 34.93	460.2 ± 27.65	2.47 ± 154.9	10.95	5.47
	304128	5.0e-4	-2.86 ± 2.70	1.45 ± 34.90	460.2 ± 27.47	2.37 ± 153.8	10.92	5.46
	304128	2.5e-4	-2.88 ± 2.72	1.47 ± 34.99	460.5 ± 27.74	2.50 ± 153.9	10.93	5.46
4	81120	9.0e-5	-5.18 ± 5.04	1.12 ± 45.10	477.0 ± 48.00	7.00 ± 223.0	10.14	4.99
	324480	2.0e-5	-4.54 ± 4.34	1.50 ± 42.50	467.5 ± 39.50	16.20 ± 188.7	10.12	5.05
5	2480814	5.1e-5	-2.88 ± 2.71	1.48 ± 35.10	463.0 ± 31.30	1.81 ± 154.0	11.00	5.50
6	7059	5.0e-4	-1.60 ± 1.60	1.50 ± 25.90	525.0 ± 22.50	-0.55 ± 106.0	10.90	5.45
	27147	5.0e-4	-2.00 ± 1.89	1.45 ± 29.00	434.0 ± 17.50	2.53 ± 88.6	10.60	5.30
7	271740	5.0e-4	-3.04 ± 2.87	1.55 ± 36.63	474.9 ± 28.12	3.86 ± 165.9	10.99	5.51

6 Summary

We have presented 2D benchmark results for different numerical approaches for fluid-structure interaction problems. These benchmarks have been developed as a collaborative project in the DFG Research Unit 493. The configurations have been carefully chosen and validated via extensive numerical tests (see also [6, 3]) with various CFD codes so that, as a main result, characteristic flow quantities can be provided which allow a quantitative validation and comparison of different numerical methods and software tools. As an extension, corresponding 3D simulations are planned as well as the embedding into outer optimization tools

(see `http://jucri.jyu.fi/?q=node/14` for a first attempt towards optimal control on the basis of the presented FSI1 configuration).

Acknowledgements The described benchmarks were developed in collaboration with G. Becker, M. Heck, S. Yigit, M. Krafczyk, J. Tölke, S. Geller, H.-J. Bungartz, M. Brenk, R. Rannacher, T. Dunne, T. Wick, W. Wall, A. Gerstenberger, P. Gamnitzer, E. Rank, A. Düster, S. Kollmannsberger, D. Scholz, M. Breuer, M. Münsch, G. De Nayer, H. Lienhart, J. Gomes, K.-U. Bletzinger, A. Kupzok, and R. Wüchner.
This work has been supported by German Research Association (DFG), Reasearch Unit 493.

References

1. P. G. Ciarlet. *Mathematical Elasticity. Volume I, Three-Dimensional Elasticity*, volume 20 of *Studies in Mathematics and its Applications*. Elsevier Science Publishers B.V., Amsterdam, 1988.
2. U. Küttler and W.A. Wall. Fixed-point fluid-structure interaction solvers with dynamic relaxation. *Computational Mechanics*, 43(1):61–72, 2008.
3. M. Razzaq, S. Turek, J. Hron, and J. F. Acker. Numerical simulation and benchmarking of fluid-structure interaction with application to hemodynamics. In *Fundamental Trends in Fluid-Structure Interaction*. World Scientific Publishing Co. Pte Ltd, 2010.
4. M. Schäfer, M. Heck, and S. Yigit. An implicit partitoned method for the numerical simulation of fluid-structure interaction. In H.-J. Bungartz and M. Schäfer, editors, *Fluid-Structure Interaction: Modelling, Simulation, Optimization*, 53, pages 171–194. Springer, Berlin, Heidelberg, 2006.
5. D.C. Sternel, M. Schäfer, M. Heck, and S. Yigit. Efficiency and accuracy of fluid-structure interaction simulations using an implicit partitioned approach. *Computational Mechanics*, 43(1):103–113, 2008.
6. S. Turek and J. Hron. Proposal for numerical benchmarking of fluid-structure interaction between an elastic object and laminar incompressible flow. In H.-J. Bungartz and M. Schäfer, editors, *Fluid-Structure Interaction: Modelling, Simulation, Optimisation*, LNCSE-53. Springer, 2006.
7. S. Turek and M. Schäfer. Benchmark computations of laminar flow around cylinder. In E.H. Hirschel, editor, *Flow Simulation with High-Performance Computers II*, volume 52 of *Notes on Numerical Fluid Mechanics*. Vieweg, 1996. co. F. Durst, E. Krause, R. Rannacher.
8. W. A. Wall and E. Ramm. Fluid-structure interaction based upon a stabilized (ALE) finite element method. In S. Idelsohn, E. Oñate, and E. Dvorkin, editors, *4th World Congress on Computational Mechanics: New Trends and Applications*, Barcelona, 1998. CIMNE.
9. W.A. Wall, D.P. Mok, and E. Ramm. Partitioned analysis approach of the transient coupled response of viscous fluids and flexible structures. In W. Wunderlich, editor, *Solids, Structures and Coupled Problems in Engineering, Proc. ECCM '99*, 1999.